Specific heat and phonon dispersion of liquid ^{4}He

Dennis S. Greywall
Bell Laboratories, Murray Hill, New Jersey 07974
(Received 23 March 1978)

The specific heat of liquid ^{4}He was measured with high precision in the temperature range from 65 to 850 mK and at sixteen molar volumes corresponding to the pressure range from vapor pressure to 25 bars. Several different analyses performed on these data yield quantitative information concerning the magnitude of the anomalous phonon dispersion as a function of pressure. The findings are generally in good agreement with the results indirectly derived from sound-propagation measurements. The specific heat data also provide precise values of the roton parameters as a function of pressure. There is an unexplained discrepancy between these values and those resulting from neutron scattering measurements.

I. INTRODUCTION

The subtle question as to whether the phonon dispersion curve of liquid ^{4}He at small momenta shows deviations from linear behavior corresponding to a positive or negative curvature has received a great deal of attention[1] over the last several years. The reason for this is that the sign of the curvature has a profound effect on the low-temperature transport properties of the liquid. If the curvature is positive, that is, if α_2 is negative in the expression

$$\epsilon = c_0 p[1 - \alpha_2(p/\hbar)^2 \cdots], \tag{1}$$

then scattering involving only three phonons is allowed at low temperatures since both energy ϵ and momentum p can be conserved. In Eq. (1), c_0 is the velocity of sound at 0 K. If, however, α_2 is positive then the three-phonon process is not allowed and the dominant scattering is via the four-phonon process. Although most experiments to date are consistent with α_2 being negative at vapor pressure, monotonically increasing as the pressure is increased, and changing sign near 18 bars, quantitative information is still unavailable.

The most direct information concerning the dispersion relation might be expected to originate from neutron scattering measurements or from sound velocity data. However, the important region of the excitation spectrum is below the momentum range where it is at present possible to make precise neutron scattering measurements and above the range where sound velocity experiments can be used to directly determine the slope of the dispersion curve. The sound velocity measurements are not possible because the mean free path of the phonons, which decreases rapidly with increasing phonon energy, becomes extremely short. It thus becomes necessary to resort to indirect methods. For example, numerical solutions[2-4] of the phonon Boltzmann equation indicate that as a result of the anomalous dispersion there is a resonant interaction between first and second sound, which leads to a small but detectable perturbation in the first-sound velocity for frequencies in the range of approximately 1–100 MHz. Thus "experimental" values[5,6] of α_2 can be inferred from a comparison of high-precision ultrasonic velocity data with curves calculated for various negative values of α_2.

Specific-heat measurements also provide indirect information concerning the dispersion relation. But the relationship between the data and the dispersion curve is, in this case, much less complicated and so one might expect the least-ambiguous results to come from such measurements. The effect to be observed in the specific heat data is, however, very small and corresponds to the determination of the deviation from T^3 behavior. This demands both extremely accurate and precise measurements which are further complicated by the fact that at low temperatures the specific heat is very small. Moreover, there is an appreciable contribution to the specific heat from the rotons for temperatures greater than approximately 0.5 K. Nonetheless, the specific heat results of Phillips *et al.*[7] were the first measurements to clearly demonstrate the existence of the anomalous phonon dispersion. Although their results are qualitatively consistent with the data inferred from the various types of sound propagation measurements, there are some serious quantitative discrepancies. These discrepancies, may be partially due to the fact that Phillips *et al.* made measurements only above 0.3 K, and thus data only over a very small temperature range were not seriously affected by the roton contribution to the specific heat.

In this paper we present new high-precision measurements of the specific heat in the temperature range from 65 to 850 mK obtained at 16 different pressures between vapor pressure and the melting curve. The data yield values of α_2, which

differ quantitatively from those determined by Phillips *et al.*[7] but are in agreement with values obtained in other experiments. Roton parameters are also derived from the specific-heat data. Although these parameters are in excellent agreement with those determined from previous thermodynamic measurements, there is an unexplained discrepancy with the neutron results. The experimental details are given in Sec. II. In Sec. III, the data and the various analyses performed on these data are discussed. A summary is provided in Sec. IV.

II. EXPERIMENTAL DETAILS

A. Calorimeter

A drawing of the calorimeter is shown in Fig. 1. The sample chamber was a short, electrodeposited-copper cylinder with hemispherical ends. The diameter of the container was 3.8 cm; the wall thickness, 0.064 cm; the mass, 40 g; and the volume, 40 cm^3. It was rigidly supported by three graphite tubes below the mixing chamber of a dilution refrigerator. The tubes were attached to the sample chamber via copper tabs which had been soft soldered to the container. Liquid helium was admitted to the chamber through an 80-cm length of quartz capillary which had an i.d. of 0.005 cm and an o.d. of 0.010 cm. The capillary was strengthened with a thin (0.003 cm) coating of extruded nylon. It was necessary to use quartz rather than, for example, stainless steel in order to reduce the heat capacity of the filling capillary to a minimum. Had a stainless-steel capillary of similar dimensions been used, its heat capacity would have been three orders of magnitude larger than that of the glass capillary and would have corresponded to approximately 25% of that of the helium sample at 50 mK and 7% at 100 mK. After being stripped of the nylon coating, the ends of the capillary were sealed into short lengths of 0.05-cm-i.d. copper tubing with epoxy. One of these pieces of copper tubing had previously been soft soldered into a nipple at the top of the cell, the other into a valve[8] mounted on the mixing chamber.

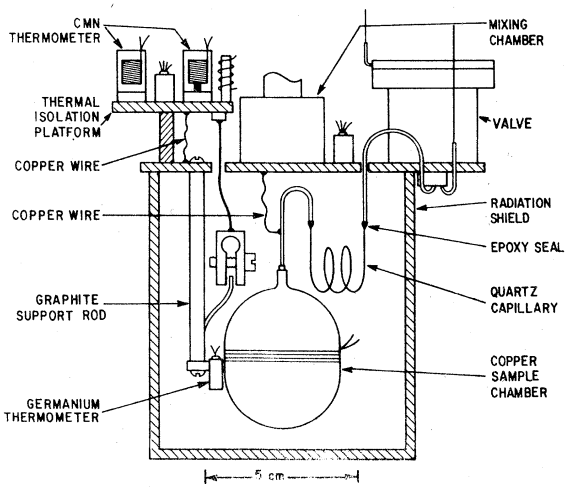

FIG. 1. Calorimeter.

The calorimeter heater, which had a nominal resistance of 10 $k\Omega$, was wound bifilarly around the cylindrical section of the cell. Platinum-tungsten (92%, 8%) resistence wire (0.0025-cm diameter) was used. Wound parallel to this heater using the same type of wire were two reference resistors (1600 Ω, 2000 Ω) and several turns of 0.0076-cm-diam copper wire which were used in heat sinking, via their leads, two germanium thermometers. The thermometer capsules (N_2 exchange gas) were mounted in thin-walled copper sleeves hard soldered to the cell support tabs. The ten leads joining the thermometers and reference resistors to the terminal strip on the mixing chamber were 0.0038-cm-diam Pt-W wires; the heater leads were 0.0076-cm-diam niobium wires.

The thermal connection between the cell and the mixing chamber was due mainly to the two niobium wires (leading to the heater), the superfluid filled capillary, and a 30-cm length of 0.0036-cm-diam copper wire. The conductions of both the niobium wires and the filled capillary increased rapidly with increasing temperature and permitted the filled calorimeter to be cooled from 0.85 K to less than 0.060 K in approximately one day. At the same time, however, the total thermal conduction at all temperatures was small relative to the magnitude of the heat capacity, and thus the specific heat could be accurately determined over the complete temperature range. The copper wire, which provided the dominant contribution to the conduction below about 0.1 K, was necessary to counter balance the 0.5 nW vibrational heat leak into the system.

During the thermometer calibration run, the cell was thermally well connected (30 μW/K at 0.1 K) to a copper platform which was in turn thermally attached (50 μW/K at 0.1 K) to the mixing chamber. On this platform, which could be temperature regulated very precisely, a cerium magnesium nitrate (CMN) thermometer, a calibrated (0.5–2.5 K) germanium thermometer, and the thermometer in the regulating circuit were mounted.

As a comment it is noted that in order to minimize the mass (and therefore the amount of vibrational heating) and also the heat capacity of the empty calorimeter, an earlier version of the sample cell was machined principally from plexiglass

(15 g). It was not, however, possible to use this chamber because of a large time-dependent heat input which presumably was emanating from the plastic itself. Twenty-four hours after cooling to low temperature, the heat leak was roughly 10 nW and was decreasing with a time constant of about 2 weeks. In amorphous and polymeric solids, the linear contribution to the low-temperature specific heat is usually attributed to the presence of a collection of two-energy-level systems. If the time constant for the establishment of thermal equilibrium, in at least some of the two-level systems, is extremely long for this plastic, then this would provide a possible explanation for the difficulty encountered in cooling this calorimeter to low temperature.

B. Thermometry

The thermometry used in this work, with only a few modifications, was the same as that described in Ref. 9. The major improvement was the replacement of the CMN tunnel-diode thermometer with a self-inductance CMN-susceptibility bridge. A thermometer of very similar design has been independently developed by R. Schweizer and H. Meyer at Duke University. The bridge circuit is shown in Fig. 2. The two 43-mH inductors were wound as identically as possible. Each coil, which had an i.d. of 0.95 cm, consisted of twelve 200-turn layers of 0.0076-cm-diam copper wire which were held in place with epoxy. One of the coils was filled with finely powdered CMN mixed with Apiezon *N* grease and 600 lengths of 0.0064-cm-diam bare copper wire. The ends of these copper wires were hard soldered[10] into a threaded copper stud. The second (reference) coil was sealed on each end with small plugs cast from epoxy and then, in the same manner as the first coil, potted in epoxy. Figure 5 of Ref. 9 is a cross-sectional drawing of a CMN thermometer constructed in a very similar fashion.

A comparison of the temperature scales determined simultaneously by the tunnel diode circuit

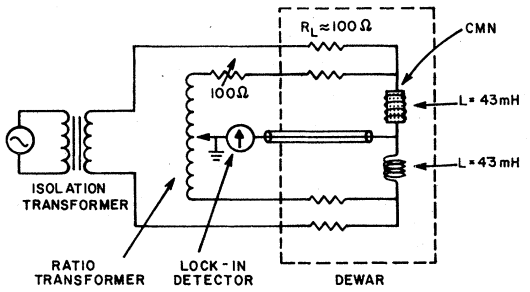

FIG. 2. Self-inductance susceptibility bridge. The bridge was normally operated at a frequency of 1 kHz.

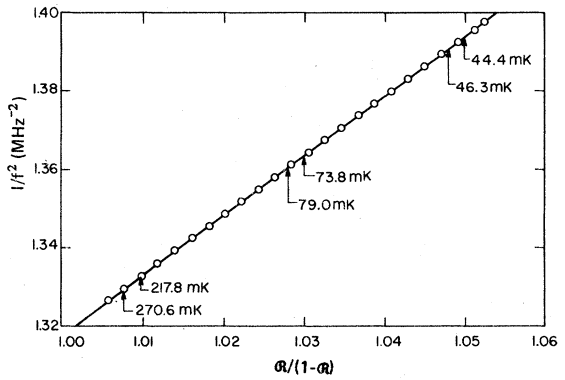

FIG. 3. Comparison of the tunnel diode and susceptibility bridge thermometers. The extremely small deviations of the data from the straight line indicate that the two scales are in excellent agreement. Other details are given in the text.

and by the susceptibility bridge (10-mH coils) is made in Fig. 3, where $1/f^2$ is plotted as a function of $\mathcal{R}/(1-\mathcal{R})$. Here f is the resonant frequency of the tunnel diode tank circuit and $\mathcal{R}$ is the bridge ratio. These two quantities should be related linearly since it can easily be shown that

$$1/T = A[\mathcal{R}/(1-\mathcal{R})] + B \tag{2}$$

and

$$1/T = C/f^2 + D\,. \tag{3}$$

In these two equations, the parameters A, B, C, and D are constants which can be determined from calibrations against the vapor pressure temperature scale of ^{3}He. The extremely small deviations from the straight line drawn through the data demonstrates that the two temperature scales corresponding to Eqs. (2) and (3) are in excellent agreement and that there are no hidden problems associated with either thermometer. With a bridge excitation voltage of 2 mV the temperature resolution was ~20 μK at 50 mK.

The parameters A and B in Eq. (2) were determined from a least-squares fitting of the calibration data shown in Fig. 4. The fit was restricted to the temperature range $0.5 < T < 1.0$ K. At higher temperatures there was an unexplained systematic deviation of the data which was accompanied by an increase in the thermal time constant. A similar deviation was also present in the data obtained with a second pair of similarly constructed coils ($L \approx 10$ mH).

The susceptibility bridge, has several obvious advantages over the tunnel diode circuit. Some of the problems with the diode circuit are (i) the voltage amplitude in the tank circuit cannot be easily varied during the course of an experiment, making it impossible to accurately determine the

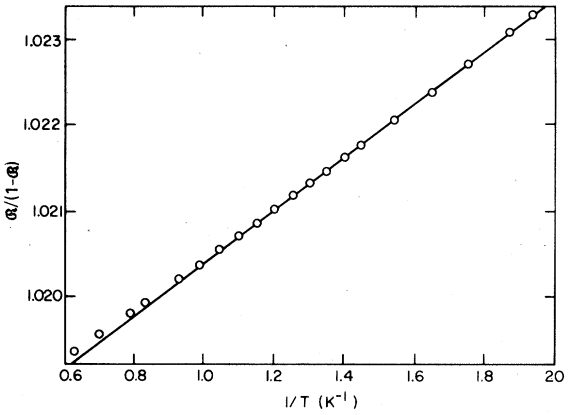

FIG. 4. CMN bridge calibration data used in determining the constants A and B in Eq. (2). Bridge frequency, 1 kHz.

amount of self-heating in the thermometer; (ii) the temperature of the diode must be kept constant; (iii) the temperature dependence of the capacitance of the coaxial cable leading from the diode to the coil can significantly affect the resonant frequency; and (iv) the high frequency (≈MHz) signal can interfere with other sensitive electronics. It was mainly for these reasons that the diode circuit was replaced by the bridge circuit.

Some comments are now made on how several design parameters in the bridge circuit were chosen. The magnetic field in the coil must be small compared to the interaction field. Thus, it is important to wind a coil with as large an inductance as reasonable and to operate the bridge at not too low a frequency. To keep the input impedance of the ratio transformer large compared to the lead resistance, however, it was necessary to restrict the frequency to the range 0.5–1 kHz. It is also important that the resistance of the coil be small compared to the reactance of the coil so that the bridge balance equations remain simple [Eq. (2)] and so that the power dissipated in the coils be small. This last condition would suggest that the coils be wound from superconducting wire. One pair of coils was wound from Nb wire but showed a strange time-dependent response to changes in the excition voltage (which may have been due to flux jumps). Therefore, copper wire was used. However, a pair of coils wound more recently from NbTi wire also worked well.

C. Number of moles of sample

Before the cell was placed in the cryostat, the copper capillary extending from the top of the sample container was joined to a gas handling system and the room-temperature volume of the cell was determined using gas-expansion measurements and a calibrated, 50-cm^3 glass volume. With the small correction (≈1%) for thermal contraction applied, the low temperature volume was determined to be 40.543 ± 0.08 cm^3. No correction was made for the pressure dependence of the volume since it was estimated to always be less than 0.1%. The number of moles of sample was calculated using this measured cell volume and the molar volume of the sample. The molar volume was determined using the pressure measured at 0.1 K (see Sec. II E) and the density-change-versus-pressure data of Abraham *et al.*[11] At vapor pressure, the molar volume was taken to be that measured by Kerr and Taylor.[12]

D. ^{4}He gas sample

Two different gas samples of ^{4}He were used in this work. Data at the first five molar volumes listed in Table I were obtained using ^{4}He purchased from Gardner Corporation. An analysis[13] of the gas indicated a ^{3}He impurity concentration of 0.37 ppm, which is about twice that normally expected for well helium. The remainder of the measurements were made using high-purity ^{4}He purchased from the U. S. Bureau of Mines.[13] The stated ^{3}He impurity level was 0.0024 ppm. However, due to the fact that the cell contained a small amount of the impure ^{4}He sample at the time the high-purity sample was condensed in the cell, the high-purity sample was contaminated with an addition amount of ^{3}He, which we estimate to be less than 0.005 ppm. Prior to use, both samples were passed through a trap at 4.2 K.

TABLE I. Pressure at 0.1 K and the molar volume (see Sec. II C) for each of the ^{4}He samples.

Sample	^{3}He Impurities (ppm)	P (bars)	V (cm^3)
1	0.370	0.09	27.550
2	0.370	2.033	26.957
3	0.370	6.021	25.978
4	0.370	4.037	26.432
5	0.370	12.164	24.852
6	0.0024	0.0	27.579
7	0.0024	2.004	26.965
8	0.0024	4.071	26.424
9	0.0024	6.031	25.976
10	0.0024	8.045	25.568
11	0.0024	10.063	25.200
12	0.0024	13.056	24.714
13	0.0024	16.143	24.273
14	0.0024	19.084	23.898
15	0.0024	22.069	23.553
16	0.0024	25.059	23.237

E. Procedure

A separate cool down of the apparatus was required in order to calibrate the two germanium thermometers on the calorimeter. This was a consequence of the necessity for keeping the heat capacity of the empty chamber to minimum. During this run the heat-switch clamp (see Fig. 1) thermally connected the calorimeter to the thermal-isolation platform. The copper wire normally joining the calorimeter directly to the mixing chamber was not in place. After completing the calibrations against the CMN thermometer, the apparatus was warmed to room temperature only long enough to remove the heat-switch clamp. With the system once again at low temperature, a partial check on the calibrations was made by comparing the two thermometers over the small temperature range (0.22–0.42 K) where the two calibrations overlapped.

The heat capacity of the empty calorimeter was now measured in the temperature interval between 0.06 and 1.8 K using the standard heat pulse technique. The detailed procedure followed in making all of the present heat capacity measurements is, with one significant modification, very similar to that described in Sec. II F of Ref. 9. In Ref. 9, the slow warming drift rate, established before the application of the heat pulse, was generated using an auxiliary heater wound on the calorimeter itself. In this work, the fore drift was a consequence of the mixing-chamber temperature being raised and precisely regulated slightly above the calorimeter temperature. For all of the heat-capacity data, the duration of the heat pulse (typically between 40 and 80 sec) and the constant current passing through the calorimeter heater were adjusted so that the resulting change in temperature was approximately 5% of T.

The calorimeter was now slowly filled with ^{4}He. Approximately 3 days were required to completely fill the chamber. It was necessary to condense the sample at a very slow rate to avoid overloading the refrigerator or warming the calorimeter to too high a temperature. Had the calorimeter been filled at $T > T_\lambda$, it would not have been possible to cool the calorimeter to low temperature in a reasonable length of time because of the extremely weak thermal link to the mixing chamber. The time required to cool the filled [at vapor pressure (VP)] calorimeter from 1 K, where the heat capacity is only about 1% of its value at T_λ, to 60 mK was about 2 days. With the cell at the desired working pressure and at a temperature of 0.1 K, the valve mounted on the mixing chamber platform was slowly closed, thereby confining the sample to constant volume. After allowing the calorimeter to cool to its lowest temperature, heat-capacity data were taken which covered the temperature range from 65 to 850 mK. Measurements were made for samples at five different molar volumes. Then, because of the large contribution to the heat capacity below 200 mK due to the unusually high ^{3}He impurity level (see Sec. II D), the gas sample was removed. After pumping on the calorimeter, which had been warmed to approximately 40 K, for several days, the chamber was flushed with high-purity gas and then pumped for several more days. After measuring the heat capacity of the empty calorimeter once again, the calorimeter was filled with the high-purity sample and the remainder of the measurements were made.

F. Heat capacity of the empty calorimeter

Due to the very long length of small-diameter filling capillary (3 m of 0.01-cm i.d. plus 0.8 m of 0.005-cm i.d.), it was not possible to completely evacuate the calorimeter. Therefore, to reduce the likelihood of a plug forming in the capillary, the calorimeter was flushed with helium gas prior to cooling the apparatus to low temperature. As a result, the measurements of the "empty"-calorimeter heat capacity showed the effects of the small residual amount of ^{4}He. The curves labeled 1, 2, and 3 in Fig. 5 were obtained 2, 6, and 7 days after the cool down to 4 K. During this time a pump was continuously attached to the capillary. For comparison, the heat capacity of a mass of copper equivalent to the mass of the calorimeter as well as the heat capacity of the ^{4}He-filled (at vapor pressure) calorimeter are shown as dashed curves. The peaks in the "empty" calorimeter curves near 1 K correspond to the vaporization of

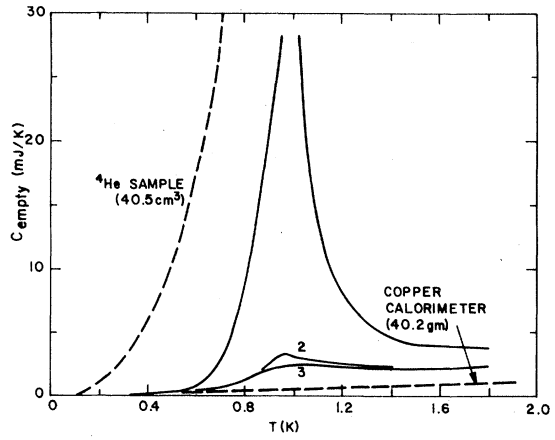

FIG. 5. Heat capacity of the "empty" calorimeter showing peaks corresponding to the vaporization of the residual amount of helium in the cell. Other details are given in the text.

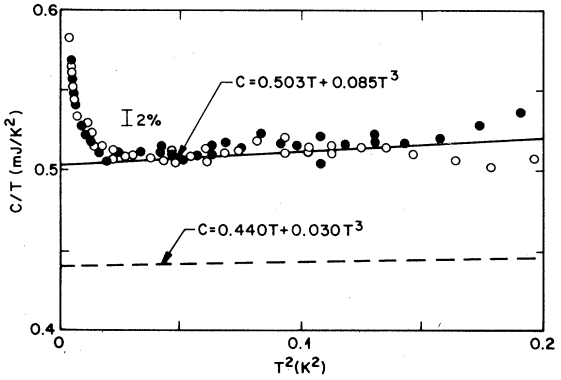

FIG. 6. Measured heat capacity of the empty calorimeter. The closed and open circles correspond, respectively, to the low temperature portion of curves 1 and 3 in Fig. 5. The dashed line is the heat capacity attributable to the copper in the calorimeter.

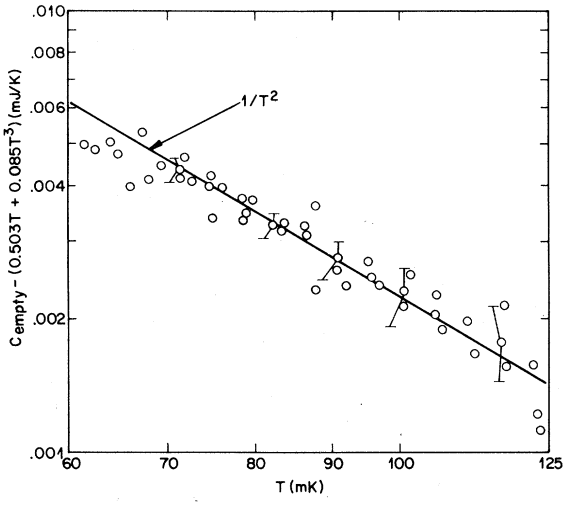

FIG. 7. $1/T^2$ contribution to heat capacity of the empty calorimeter.

the small amount of helium in the cell. The temperature at which the peaks occur and the heat capacity in the nearly temperature-independent region above approximately 1.4 K each indicate that the cell contained roughly 10^{-4} moles of helium. The decrease in the peak height with time is an indication that the amount of helium being removed from the cell at low temperature was not negligible. This was due to the helium being carried up into the large diameter capillary leading out of the Dewar via film flow.

In Fig. 6, the data of curves 1 and 3 in Fig. 5 are plotted as C/T vs T^2 for $T^2 < 0.2$ K^2 ($T \lesssim 0.45$ K). For $0.03 < T^2 < 0.2$ K^2 the effect of the residual helium is negligible, and the data for both runs can be described well by the straight line drawn through the data corresponding to a function of the form $AT + BT^3$, as expected. At higher temperatures the contribution due to the vaporization of the residual helium becomes appreciable while at lower temperatures another contribution to the heat capacity becomes significant. In Fig. 7 the measured heat capacity below 125 mK (from four different runs), minus the terms going as T and as T^3, is plotted as a function of temperature on log-log scales. At 50 mK, this term accounts for about $\frac{1}{3}$ of the heat capacity. The results are well represented by D/T^2 with $D = 2.3 \times 10^{-5}$ mJ K. If this contribution is attributed to the copper, then $D = 3.6 \times 10^{-5}$ mJ K/mole. This value is in excellent agreement with the findings of Sellers and Anderson[14] from their low-temperature heat capacity measurements on annealed copper. The source of this term in the copper is, however, unknown.

The dashed line in Fig. 6 gives the expected contribution to the empty calorimeter heat capacity from the copper (neglecting the $1/T^2$ term). The difference between the two lines is due to contributions from other materials in the calorimeter. Some of these contributions are shown in Fig. 8. Since a sizable portion of the empty calorimeter heat capacity is not accounted for, a large contri-

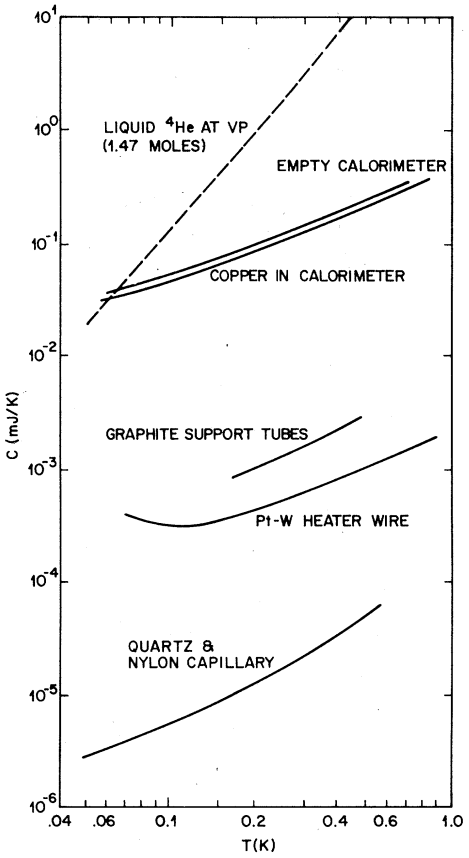

FIG. 8. Contributions to the heat capacity of the empty calorimeter.

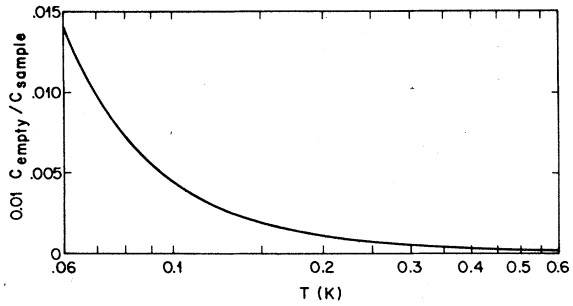

FIG. 9. Uncertainty in the sample heat capacity (at vapor pressure) due to a 1% uncertainty in the empty calorimeter heat capacity.

bution must be attributed to the germanium thermometers, the varnish (GE7031) holding down the heater, small amounts of soft and hard solder, and the epoxy capillary seal. We note that the magnitude of the heat capacity in excess of the copper is roughly the same as that found for the more massive calorimeter used previously[8] for measurements on bcc ^{3}He.

The error bars shown in Fig. 7 correspond to an estimate of the uncertainty in the measurements due only to possible errors in the extrapolations of the before and after drifts to the center of the heating interval. These errors are relatively large for the empty calorimeter because of the small heat capacity; a small heat capacity implies a fast drift rate. At the lowest temperatures the error from this source is about $\pm\frac{1}{2}\%$. With increasing temperature the drift rate and thus also the error increases; at 0.6 K the errors are of the order of 1%. The uncertainty in the helium sample heat capacity, due only to this source of error, is shown in Fig. 9. For this calculation a constant uncertainty in the empty of 1% was assumed.

III. RESULTS AND DISCUSSION

A. Specific-heat data

The specific heat of liquid ^{4}He was measured at the 16 molar volumes listed in Table I. The data cover the temperature range from 65 to 850 mK and the pressure range from 0 to 25 bars. Samples 1–5 had a ^{3}He impurity concentration of 0.37 ppm; the remainder of the samples had 0.0024-ppm ^{3}He. In Fig. 10 the results for two of the high-purity samples are shown on a log-log plot. The data obtained at vapor pressure (sample 6) are plotted as open circles; the data at approximately 22 bars (sample 15) are plotted as closed circles. Below approximately 0.5 K the results at both pressures fall along straight lines corresponding to the nearly-T^3 temperature dependence expected for the

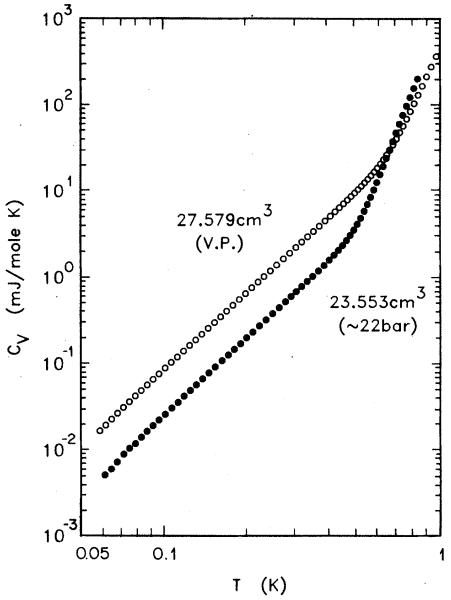

FIG. 10. Specific heat of liquid ^{4}He obtained at two molar volumes.

phonon contribution to the specific heat. At higher temperatures the roton contribution, becomes significant. This latter contribution becomes appreciable at lower temperature for the 22 bars data since the roton energy gap decreases with increasing pressure.

In order to present the results in a much more sensitive manner, all of the data are plotted as C_V/T^3 vs T^2 in Figs. 11 and 12. A straight line in these figures corresponds to a specific heat that can be described by the function AT^3+CT^5. The intercept of the line on the C_V/T^3 axis gives the coefficient A; C is given by the slope of the line. All of the data shown in Figs. 11 and 12 can be described reasonably well by straight lines for $0.05 \lesssim T^2 \lesssim 0.15$ K^2. The deviations at higher temperatures correspond mainly to the roton contribution to the total specific heat. The very-sharply-increasing deviations shown in Fig. 11 for $T^2 \lesssim 0.05$ K^2 can be explained as being mainly due to the nearly constant specific heat attributable to the ^{3}He impurities. The more subtle deviations of the high-purity data plotted in Fig. 12 for $T^2 < 0.05$ K^2 are more difficult to explain. It is assumed that none of this effect is attributable to the real specific heat of liquid ^{4}He. There are several possible sources of experimental difficulties to examine: (i) an improper thermometer calibration, (ii) errors in the empty calorimeter heat capacity, and (iii) a ^{3}He impurity level much higher than expected. Since the measurements were made at several different pressures however, the latter two possibilities can immediately be ruled out as

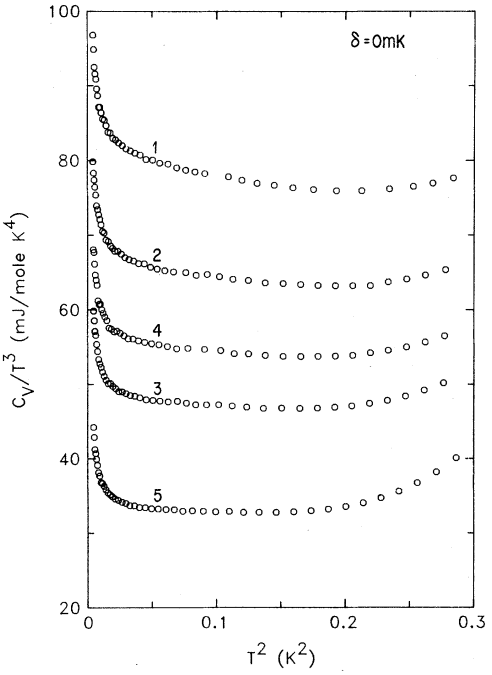

FIG. 11. Specific heat of samples 1–5. The data were determined using a thermometer calibration based on $T^* = T$.

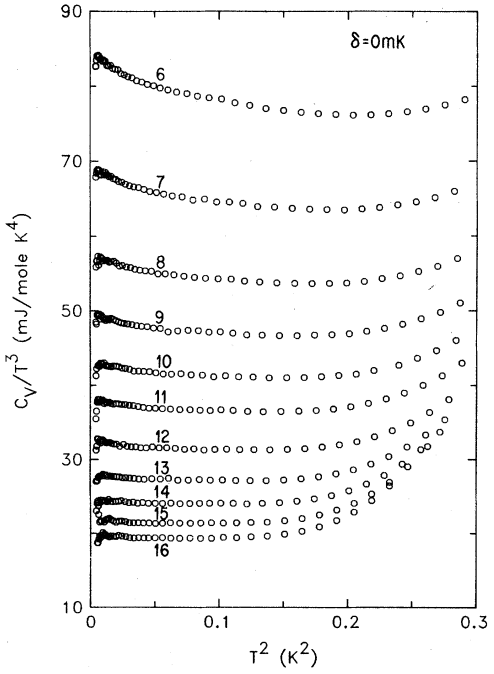

FIG. 12. Specific heat of samples 6–16. The data were determined using a thermometer calibration based on $T^* = T$.

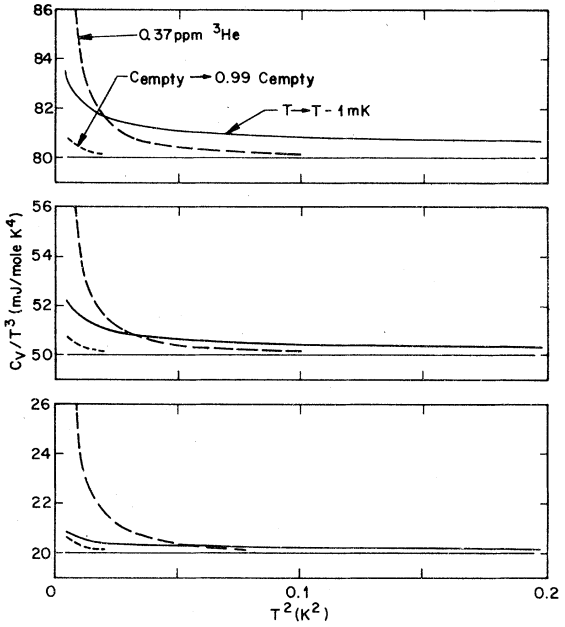

FIG. 13. Effects on the ^{4}He specific-heat measurements due to several possible experimental difficulties. Other details are given in the text.

not being sources of significant error. In Fig. 13, the effects of a uniform shift in the temperature scale of 1 mK, a decrease in the empty cell heat capacity of 1%, and a ^{3}He impurity concentration of 0.37 ppm are shown, respectively. Since the results of these computations are again plotted as C/T^3 vs T^2 a direct comparison can be made with Figs. 11 and 12. Note, however, that in plotting Fig. 13 it was assumed that the "real" specific heat is proportional to T^3 (i.e., that $C = 0$), which corresponds to a horizontal line in this type of plot. The calculations were made with T^3 coefficients of 80, 50, and 20 mJ/K^4. These values correspond approximately to the results obtained near 0, 6, and 25, bars, respectively. As explicitly shown in the figure, an error in the determination of the empty calorimeter heat capacity or the presence of ^{3}He impurities would manifest itself as a nearly-pressure-independent deviation from the actual sample heat capacity. This is in contrast to an error in the temperature scale which leads to deviations proportional to the heat capacity and, at least qualitatively, consistent with the observations. One possible explanation for an error in the temperature scale is that on thermal cycling the calibrations of the resistance thermometers shifted. However, the size of the shift necessary to explain the observations is much larger than we would expect based on several calibrations of these particular thermometers after repeated thermal

cycling, including one made at the completion of the experiment. It is also difficult to attribute the problem to an error in the high-temperature (>0.5 K) calibration of the CMN thermometer (against which the resistance thermometers were in turn calibrated), since an incorrect determination of the slope of the susceptibility-versus-$1/T$ line would imply that $\delta T/T \approx$ const; a simple scaling of the temperature would not alter the functional form describing the data. Another possible source of error in the temperature scale is due to the fact that the CMN thermometer actually determines $T^* \equiv T - \delta$. It is often assumed that δ is much less than 1 mK. The constant δ, however, depends on the details of the thermometer construction, and a value as large as 2 mK for our relatively long coil is not inconsistent with other determinations.[15,16] Shown in Fig. 14 are the C_V data at vapor pressure determined using thermometer calibrations based on δ equal to 0, 1, 2, and 3 mK. With $\delta = 2$ mK, the range over which the data can be described well by a straight line is extended on the low-temperature end to approximately 0.01 K^2. The data for each of the high-purity samples, determined with the $\delta = 2$ mK calibration, are shown in Fig. 15. At each of the pressures, the results with $0.01 \lesssim T^2 \lesssim 0.15$ K^2 are well described by a straight line. The nearly pressure-independent deviations below $T = 0.01$ K^2 are within the experimental uncertainty. They could be due to an error in the empty cell heat capacity of about 1%. It is also probable that at least a portion of the deviation for each sample is due to errors in the measurements associated with the relatively fast temperature drift rates corresponding to the very small sample heat capacity at low temperatures.

Direct comparison with other high-precision measurements is extremely limited since only the data of Phillips *et al.*[7] overlap with our temperature range. These data extend down in temperature to 0.3 K and agree with our results to within

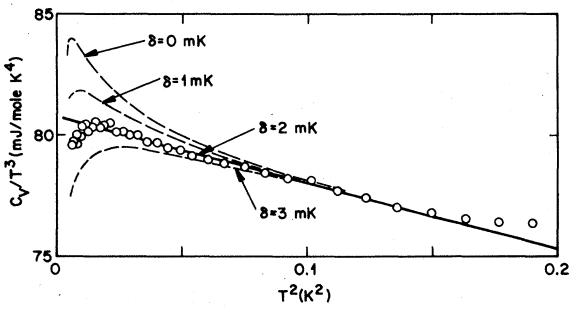

FIG. 14. ^{4}He specific heat at vapor pressure (sample 6) determined using thermometer calibrations based on $T^* = T - \delta$, with $\delta = 0$, 1, 2, and 3 mK.

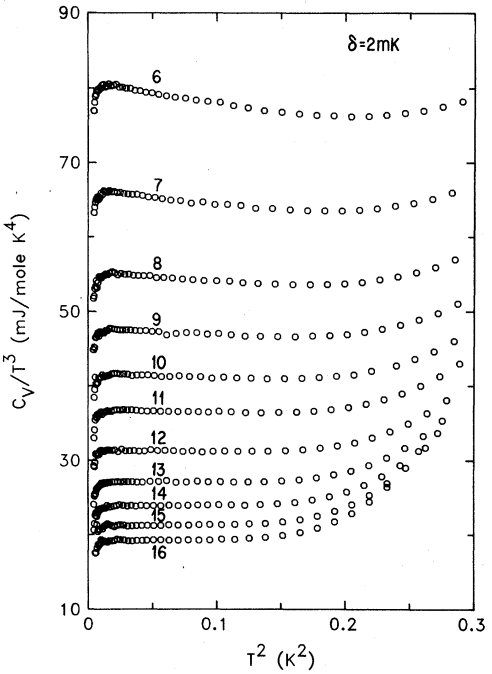

FIG. 15. Specific heat of samples 6–16. The data were determined using a thermometer calibration based on $T^* = T - 2$ mK.

about 3%. To be noted, (See Fig. 10) most of the data of Ref. 7 are at a high enough temperature to be significantly affected by the roton contribution.

B. Anomalous phonon dispersion

The principal concern in this section is with the phonon contribution to the specific heat and in particular with the deviations of the specific heat, from an extrapolation of the asymptotic T^3 behavior. A normal energy-momentum (ϵ,p) phonon dispersion curve is one that curves downward, i.e. for $p > 0$, $\epsilon < c_0 p$, where c_0 is the long wavelength sould velocity. This type of dispersion relation implies that the deviations of the specific heat from the limiting T^3 behavior should be positive. This is, however, contrary to the results shown in Figs. 11, 12, and 15. Here, the data at low pressures show definite negative deviations (from horizontal straight lines passing through an extrapolation of the data to $T^2 = 0$), implying an anomalous upward curving phonon dispersion in qualitative agreement with other previous experiments on liquid ^{4}He.

In order to make this discussion more quantitative it is assumed that the phonons are noninteracting and, that for small phonon momenta, the dispersion relation can be written as

$$\epsilon = c_0 p[1 - \alpha_1(p/\hbar) - \alpha_2(p/\hbar)^2 - \alpha_3(p/\hbar)^3 - \alpha_4(p/\hbar)^4 - \ldots]. \quad (4)$$

High-precision ultrasonic measurements[17] have indicated that $\alpha_1 \approx 0$ at vapor pressure. To simplify Eq. (4) somewhat, the assumption was made that $\alpha_1 \equiv 0$ at all pressures. It then follows from a straightforward Debye-type calculation that the low-temperature phonon specific heat is given by the expression

$$C_V^{\text{phonon}} = AT^3 + CT^5 + DT^6 + ET^7 + \ldots , \tag{5}$$

with

$$A = 4\pi R/5\theta^3 ,$$

$$C = (25/7)\alpha_2 A(2\pi k_B/\hbar c_0)^2 ,$$

$$D = 4.732\alpha_3 A(2\pi k_B/\hbar c_0)^3 ,$$

$$E = 7(4\alpha_2^2 + \alpha_4)A(2\pi k_B/\hbar c_0)^4 ,$$

where

$$\theta \equiv (\hbar c_0/k_B)(6\pi^2 N/V)^{1/3} ,$$

R is the gas constant, k_B is Boltzmann's constant, and N is Avogadro's number.

A second contribution to the total specific heat, which can be considered separately and which becomes significant above a few tenths of a degree, is due to the excitations near the minimum in the ^{4}He dispersion curve, i.e., the rotons. The energy-momentum relation for this region of the dispersion curve is approximated by

$$\epsilon = \Delta + (p - p_0)^2/2\mu , \tag{6}$$

where Δ is the energy gap, p_0 is the position of the energy minimum, and μ is the effective mass of the roton. Equation (6) implies that the roton contribution to the molar specific heat is

$$C_V^{\text{roton}} = F(\Delta/k_B T)^{3/2} \times [1 + k_B T/\Delta + \tfrac{3}{4}(k_B T/\Delta)^2] e^{-\Delta/k_B T} , \tag{7}$$

where

$$F = 2Vk_B \mu^{1/2} p_0^2 \Delta^{1/2}/(2\pi)^{3/2}\hbar^3 .$$

Since the contributions[18] from other parts of the spectrum are negligible over the temperature range in which the present data were obtained, the total specific heat can be taken to be simply the sum of the phonon and roton terms,

$$C_V = C_V^{\text{phonon}} + C_V^{\text{roton}} . \tag{8}$$

The specific-heat data were least-squares fitted in various ways using Eq. (8). In all cases the data corresponding to the $\delta = 2$-mK thermometer calibration were used in order to be consistent with the assumption $\alpha_1 \equiv 0$ [or equivalently $BT^4 \equiv 0$ in Eq. (5)].

Analysis 1. The first fitting of the high-purity data at each of the molar volumes was performed with only A and C as adjustable parameters. D and E were held fixed at zero; the roton parameters Δ and F were fixed at values determined using neutron data[19] obtained at 1.3 K. The fits covered a temperature range $T_{\min} < T < T_{\max}$ in which the rotons provided at most a 0.5% contribution to the total specific heat. See Fig. 16. $T_{\min}$ was also a function of the sample molar volume and was chosen so that a 0.5% uncertainty in the empty calorimeter heat capacity would correspond to less than a 0.1% uncertainty in the specific heat of the samle for $T > T_{\min}$. Results of the fits are listed in Table II. The uncertainties given for the parameters are statistical errors. In Fig. 17 the values of α_2, derived from the best-fit values of C using Eq. (5), are plotted (open circles) as a function of sample pressure. The parameter α_2 is equal to -0.74 Å^2 at vapor pressure and increases, nearly linearly, with increasing pressure, becoming positive (normal dispersion) at approximately 16 bars. The pressure at which α_2 changes sign, that is, the pressure above which the phonon dispersion is normal, is somewhat lower than, but in reasonable agreement with, the results from various sound propagation experiments. The phonon beam spreading measurements of Sherlock *et al.*[20] indicate that the crossover pressure is ~17 bars; the high-precision sound velocity measurements of Junker and Elbaum[6] yield a crossover pressure of ~18 bars; and the ultrahigh-frequency sound attenuation measurements of Dynes and Narayanamurti[21] imply that the phonon dispersion is normal above ~20 bars. The present results, however, conflict with the critical pressure determined by Phillips *et al.*[7] The analysis of these specific heat

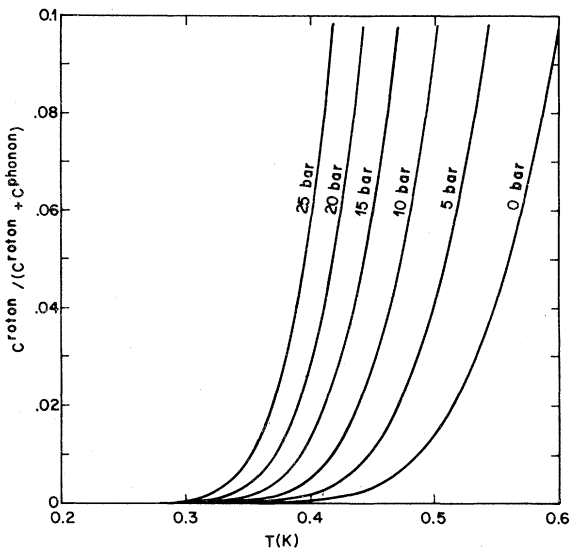

FIG. 16. Relative contribution of the rotons to the total specific heat of liquid ^{4}He.

TABLE II. Results of least-squares fits of the specific heat data with the expression $C_V = AT^3 + CT^5 + DT^6 + ET^7 + F f(T/\Delta)$. The function $f(T/\Delta)$ is defined in Eq. (7). The quantities c_0, α_2, α_3, α_4, and $\mu^{1/2} p_0^2$ are related to the parameters in the above expression via Eqs. (5) and (7).

Sample	T_{min} (K)	T_{max} (K)	A (mJ/mole K^4)	C (mJ/mole K^6)	D (mJ/mole K^7)	E (mJ/mole K^8)	$F/10^4$ (mJ/mole K)	Δ/k_B (K)	c_0 (m/sec)	α_2 (Å^2)	α_3 (Å^3)	α_4 (Å^4)	$\left(\frac{\mu}{m_4}\right)^{1/2}\left(\frac{P_0}{\hbar}\right)^2$ (Å^{-2})	rms (%)
Analysis 1: Adjustable parameters: A, C; Fixed parameters: D, $E = 0$; F, Δ = values from neutron data (1.3 K).														
6	0.140	0.460	80.64 ± 0.07	−24.9 ± 0.7	0	0	5.70	8.61	240.6	−0.74	0	–	1.4	0.22
7	0.149	0.450	66.19 ± 0.06	−16.3 ± 0.6	0	0	5.52	8.45	255.1	−0.66	0	–	1.4	0.22
8	0.159	0.435	55.22 ± 0.04	−10.7 ± 0.4	0	0	5.37	8.30	269.2	−0.58	0	–	1.4	0.15
9	0.166	0.420	47.68 ± 0.06	−7.2 ± 0.6	0	0	5.23	8.16	281.1	−0.49	0	–	1.4	0.22
10	0.174	0.405	41.62 ± 0.04	−4.8 ± 0.4	0	0	5.10	8.02	292.5	−0.41	0	–	1.4	0.15
11	0.180	0.395	36.82 ± 0.03	−3.0 ± 0.4	0	0	4.99	7.89	303.3	−0.31	0	–	1.4	0.13
12	0.190	0.380	31.40 ± 0.05	−1.4 ± 0.6	0	0	4.83	7.70	317.7	−0.19	0	–	1.4	0.20
13	0.200	0.370	27.20 ± 0.07	−0.8 ± 0.8	0	0	4.69	7.52	331.3	−0.07	0	–	1.4	0.18
14	0.210	0.360	23.87 ± 0.05	+1.2 ± 0.6	0	0	4.57	7.36	344.3	+0.24	0	–	1.4	0.18
15	0.218	0.350	21.17 ± 0.05	+1.7 ± 0.5	0	0	4.46	7.21	356.6	+0.42	0	–	1.4	0.14
16	0.225	0.340	19.26 ± 0.05	+0.5 ± 0.6	0	0	4.35	7.07	366.4	+0.13	0	–	1.4	0.18
Analysis 2: Adjustable parameters: A, C, E, F, Δ; Fixed parameters: $D = 0$.														
6	0.140	0.86	81.19 ± 0.04	−40.1 ± 0.8	0	73 ± 3	6.82 ± 0.10	8.80 ± 0.02	240.1	−1.18	0	3.86	1.66	0.10
7	0.149	0.85	66.61 ± 0.04	−28.2 ± 0.7	0	60 ± 3	6.73 ± 0.09	8.68 ± 0.02	254.6	−1.13	0	6.57	1.68	0.10
8	0.159	0.83	55.54 ± 0.04	−19.4 ± 0.7	0	45 ± 2	6.55 ± 0.07	8.54 ± 0.01	268.7	−1.04	0	8.92	1.68	0.08
9	0.166	0.82	47.92 ± 0.06	−13.8 ± 1.1	0	35 ± 4	6.39 ± 0.11	8.42 ± 0.02	280.6	−0.94	0	10.79	1.68	0.16
10	0.174	0.80	41.77 ± 0.05	−9.3 ± 0.9	0	26 ± 4	6.17 ± 0.09	8.28 ± 0.02	292.2	−0.78	0	11.45	1.67	0.13
11	0.180	0.79	36.97 ± 0.04	−7.0 ± 0.7	0	23 ± 3	6.09 ± 0.06	8.18 ± 0.01	302.9	−0.72	0	14.34	1.68	0.10
12	0.190	0.77	31.51 ± 0.06	−4.4 ± 1.1	0	18 ± 5	5.85 ± 0.09	8.01 ± 0.02	317.4	−0.59	0	16.69	1.66	0.14
13	0.200	0.75	27.32 ± 0.07	−4.0 ± 1.3	0	18 ± 5	5.69 ± 0.08	7.85 ± 0.02	330.8	−0.66	0	22.50	1.66	0.16
14	0.210	0.74	23.91 ± 0.06	+0.3 ± 1.1	0	3 ± 5	5.44 ± 0.06	7.67 ± 0.01	344.1	+0.06	0	6.06	1.63	0.13
15	0.218	0.72	21.24 ± 0.06	+0.4 ± 1.2	0	6 ± 6	5.32 ± 0.06	7.52 ± 0.01	356.2	+0.10	0	13.72	1.64	0.13
16	0.225	0.71	19.35 ± 0.05	−2.3 ± 1.0	0	21 ± 5	5.28 ± 0.04	7.41 ± 0.01	365.8	−0.67	0	58.24	1.66	0.11
Analysis 3: Adjustable parameters: A, C, E, F; Fixed parameters: $D = 0$, Δ = values from neutron data (extrapolated to 0 K).														
6	0.140	0.86	81.08 ± 0.05	−37.3 ± 0.7	0	62 ± 2	6.39 ± 0.04	8.71	240.2	−1.10	0	3.08	1.56	0.12
7	0.149	0.85	66.50 ± 0.04	−25.2 ± 0.7	0	47 ± 2	6.34 ± 0.03	8.60	254.7	−1.02	0	5.07	1.59	0.13
8	0.159	0.83	55.43 ± 0.04	−16.6 ± 0.6	0	33 ± 2	6.15 ± 0.03	8.46	268.8	−0.90	0	6.45	1.59	0.12
9	0.166	0.82	47.79 ± 0.06	−10.7 ± 0.9	0	22 ± 3	6.03 ± 0.04	8.34	280.8	−0.73	0	6.63	1.60	0.19
10	0.174	0.80	41.58 ± 0.06	−4.5 ± 1.0	0	3 ± 3	5.60 ± 0.03	8.16	292.6	−0.38	0	1.17	1.52	0.20
11	0.180	0.79	36.65 ± 0.08	+0.5 ± 1.3	0	−12 ± 4	5.38 ± 0.03	8.02	303.7	+0.05	0	− 8.64	1.50	0.27
12	0.190	0.77	31.16 ± 0.09	+3.6 ± 1.5	0	−20 ± 5	5.13 ± 0.04	7.85	318.5	+0.48	0	− 21.64	1.47	0.29
13	0.200	0.75	26.86 ± 0.11	+6.5 ± 1.9	0	−32 ± 7	4.96 ± 0.05	7.68	332.7	+1.10	0	− 50.57	1.47	0.36
14	0.210	0.74	23.49 ± 0.10	+9.9 ± 1.6	0	−43 ± 6	4.83 ± 0.04	7.53	346.1	+2.08	0	− 100.3	1.46	0.31
15	0.218	0.72	20.64 ± 0.14	+13.3 ± 2.3	0	−57 ± 9	4.76 ± 0.04	7.38	359.6	+3.45	0	− 192.9	1.48	0.40
16	0.225	0.71	18.58 ± 0.17	+15.1 ± 2.9	0	−67 ± 11	4.51 ± 0.05	7.22	370.8	+4.61	0	− 299.2	1.44	0.49

TABLE II. (*Continued*)

Sample	T_{min} (K)	T_{max} (K)	A (mJ/mole K^4)	C (mJ/mole K^6)	D (mJ/mole K^7)	E (mJ/mole K^8)	$F/10^4$ (mJ/mole K)	Δ/k_B (K)	c_0 (m/sec)	α_2 (Å^2)	α_3 (Å^3)	α_4 (Å^4)	$\left(\frac{\mu}{m_4}\right)^{1/2}\left(\frac{p_0}{\hbar}\right)^2$ (Å^{-2})	rms (%)
Analysis 4: Adjustable parameters: A, C, E, F, Δ; Fixed parameters: D = theoretical values [Eq. (12)].														
6	0.140	0.86	81.37 ± 0.05	-52.8 ± 0.9	50.89	19 ± 4	7.02 ± 0.10	8.79 ± 0.02	239.9	-1.55	+3.28	-7.13	1.71	0.11
7	0.149	0.85	66.73 ± 0.04	-36.1 ± 0.8	31.90	25 ± 3	6.83 ± 0.09	8.67 ± 0.02	254.4	-1.45	2.99	-3.50	1.71	0.10
8	0.159	0.83	55.61 ± 0.03	-24.5 ± 0.6	20.71	23 ± 3	6.61 ± 0.07	8.54 ± 0.01	268.5	-1.31	2.74	-0.29	1.70	0.09
9	0.166	0.82	47.97 ± 0.06	-17.5 ± 1.2	14.68	19 ± 5	6.44 ± 0.11	8.42 ± 0.02	280.5	-1.19	2.57	2.23	1.70	0.16
10	0.174	0.80	41.82 ± 0.05	-11.9 ± 0.9	10.70	14 ± 4	6.20 ± 0.09	8.28 ± 0.02	292.1	-1.00	2.42	3.39	1.67	0.13
11	0.180	0.79	37.00 ± 0.04	-9.0 ± 0.7	7.99	14 ± 3	6.11 ± 0.06	8.18 ± 0.01	302.8	-0.92	2.27	6.69	1.68	0.10
12	0.190	0.77	31.53 ± 0.06	-5.8 ± 1.1	5.53	12 ± 5	5.86 ± 0.09	8.01 ± 0.02	317.3	-0.77	2.12	9.42	1.67	0.14
13	0.200	0.75	27.34 ± 0.08	-5.0 ± 1.3	3.94	13 ± 5	5.70 ± 0.08	7.85 ± 0.02	330.7	-0.82	1.98	15.46	1.67	0.16
14	0.210	0.74	23.92 ± 0.06	-0.4 ± 1.1	2.89	0 ± 5	5.44 ± 0.06	7.67 ± 0.01	344.0	-0.08	1.86	.01	1.63	0.13
15	0.218	0.72	21.25 ± 0.06	-0.1 ± 1.2	2.18	3 ± 6	5.32 ± 0.06	7.52 ± 0.01	356.2	-0.03	1.76	7.90	1.64	0.13
16	0.225	0.71	19.36 ± 0.05	-2.8 ± 1.0	1.75	19 ± 5	5.29 ± 0.05	7.41 ± 0.01	365.7	-0.79	1.68	51.56	1.66	0.12

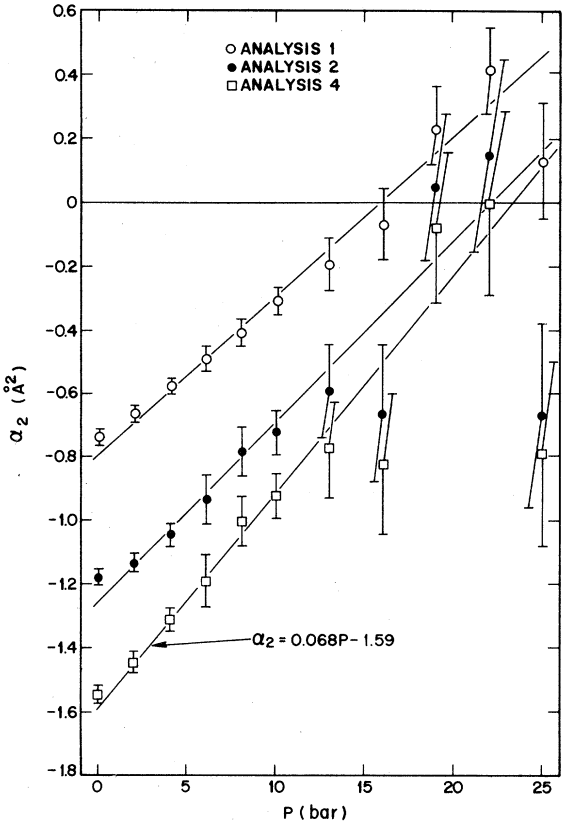

FIG. 17. α_2 resulting from three different analyses of the data (see text) plotted as a function of pressure. The straight lines correspond to least squares fits of the α_2-P data (the points at 25 bars were not included).

data implies that $P_c \approx 8$ bars. The comparisons of the magnitudes of α_2 at vapor pressure are more complicated. Phillips *et al.*[7] find $\alpha_2 = -0.46$ Å^2, but we note again that their results are based on an analysis of C_V data obtained only above 0.3 K. When an analysis identical to that used by Phillips *et al.*[7] was performed on the present vapor pressure data in the temperature range from 0.3 to 0.95 K (F and Δ as well as A and C floating parameters) we obtained $\alpha_2 = -0.42$ Å^2, in excellent agreement with their value. The fact that this significantly different value of α_2 is obtained when a fit is performed over this higher range of temperatures demonstrates that it is very difficult to obtain accurate values of α_2 from C_V data that do not extend considerably below 0.3 K. It also indicates that a more complicated function will be required to properly fit the data over a temperature range which extends to these higher temperatures. A value of $\alpha_2 = -1.7 \pm 0.34$ Å^2 has been obtained from thermal expansion measurements by Berthold *et al.*[22] The analysis of these data is complicated by the fact that the density dependence of the various

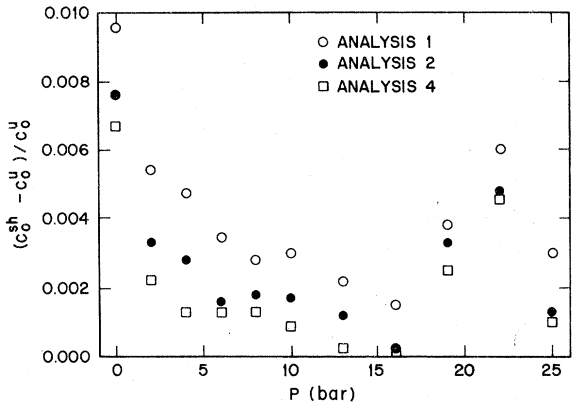

FIG. 18. A comparison of the sound velocities derived from the specific heat data (c_0^{sh}) with the directly measured (Ref. 11) ultrasonic values (c_0^u).

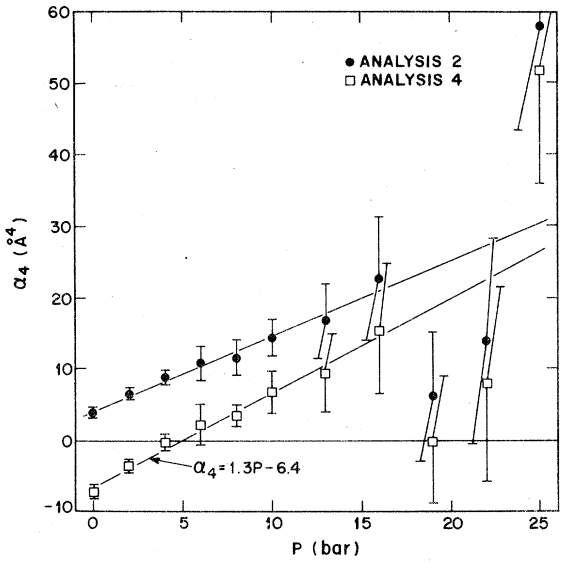

FIG. 19. α_4 resulting from two different analyses of the data (see text) plotted as a function of pressure. The straight lines correspond to least squares fits of the α_4-P data for $P \leq 16$ bars.

parameters must enter the analysis. The comparison with their value is not really justified at this point since in their analysis of the data $\alpha_3 \neq 0$ but was instead fixed to agree with theory (see analysis 4). Values of α_2 can be derived from sound velocity[5,6] and attenuation[23] measurements only within the framework of a theoretical model and vary considerably depending on the particular calculation[2-4] to which comparison is made. These indirectly determined values of α_2 fall in the range from -2.0 to -1.1 Å^2.

Figure 18 compares the sound velocities, derived [Eq. (5)] from the best-fit values of A with the directly measured velocities.[11] Except at $P=0$, the discrepancy is of the order of several tenths of a percent and is not unreasonable. The smoothed values of the ultrasonic velocities used for the comparison may be in themselves in error by a few tenths of a percent. The systematic errors in the velocities derived from the specific heat data are expected to be due mainly to the uncertainty in the cell volume and to errors in the temperature scale. At $P=0$ the larger discrepancy would be explained if the calorimeter was slightly overfilled.

Analysis 2. In this set of fits A, C, E, F, and Δ were all treated as adjustable parameters; D was held fixed at zero. The low cutoff temperature T_{min} for each of the samples was the same as in analysis 1; however, the temperature range over which the data were fitted was greatly increased by raising T_{max} to approximately $\Delta(P)/10$. The results are listed in Table II. Fits of the data obtained at vapor pressure (sample 6) were also made using several different values of T_{max} to further test the suitability of this fitting function. For $0.75 \leq T_{max} \leq 0.95$ K there were no significant differences in any of the resulting, respective best-fit parameters. For smaller values of T_{max} it was, as expected, the roton parameters F and Δ that were most affected. The values of c_0, α_2, and α_4 for each of the samples derived from the best-fit parameters A, C, and E are also listed in Table II and are plotted in Figs. 18, 17, and 19, respectively, as solid circles. Compared to analysis 1, the sound velocities show an improved agreement with the ultrasonic data. The values of α_2 determined in this analysis fall systematically below those of the first analysis by roughly 0.4 Å^2. This demonstrates that even for temperatures less than a few tenths of a degree, the contribution to the specific heat resulting from the T^7 term is significant and thus that a fitting function which includes adjustable terms of higher order than T^5 is required to adequately fit the data.

This second analysis of the data implies that the phonon dispersion should become normal near 20 bars, in close agreement with the P_c determined by Dynes and Narayanamurti.[21] These authors measured, as a function of pressure, the cutoff energy ϵ_c below which a high-frequency phonon can spontaneously decay via the three-phonon process. They found that ϵ_c goes to zero at about 20 bars. Recall that the three-phonon process is not allowed for a phonon dispersion that is normal for all momenta. A further comparison of the two experiments can be made at lower pressures since the critical wave vector k_c corresponding to ϵ_c is related to α_2 and α_4 by

$$k_c^2 = -4\alpha_2/5\alpha_4 \ . \qquad (9)$$

Dynes and Narayanamurti found that $k_c \approx 0.5$ Å^{-1} at

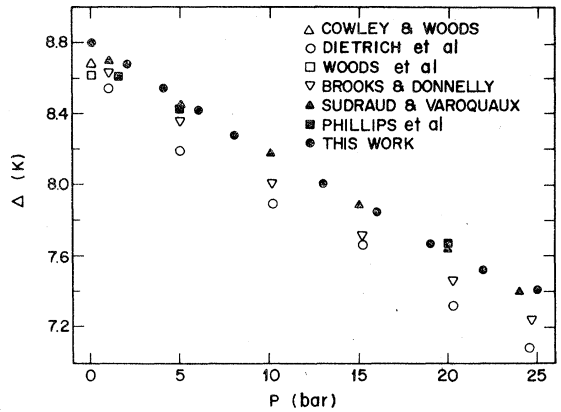

FIG. 20. Roton energy gap vs pressure. The open symbols correspond to neutron scattering values [Cowley and Woods (Ref. 26); Dietrich *et al.* (Ref. 19); Woods *et al.* (Ref. 27); Brooks and Donnelly (Ref. 28)]; the closed symbols to thermodynamic results [Phillips *et al.* (Ref. 7); Sudraud and Varoguaux (Ref. 29)]. Other details are given in the text.

$P=0$ and decreases linearly to 0 at 20 bars. At $P=0$ we also find via Eq. (9) $k_c \approx 0.5$ Å^{-1}. At intermediate pressures the present analysis yields values of k_c roughly 25% smaller than those determined by the direct measurements. This difference is probably still within the combined experimental uncertainties, and it is therefore concluded that the two experiments are consistent. These numbers are also in reasonable agreement with the values deduced by Jackle and Kehr,[24] using ultrasonic data.[25]

In Figs. 20 and 21, the roton parameters Δ and $\mu^{1/2}p_0^2$ [derived from F using Eq. (7)] are shown and compared with results from other experiments. The open symols correspond to neutron data by Cowley and Woods[26] obtained at 1.1 K, by Dietrich *et al.*[19] obtained at 1.3 K, and by Woods *et al.*[27] obtained at 0.75 K. Zero-temperature extrapolations of the smoothed neutron data[19,26] by Brooks and Donnelly[28] are also indicated. The closed symbols refer to low-temperature thermodynamic results.[7,29] There is an obvious discrepancy of about 0.2 K between the two types of measurements which is considerably outside of the combined experimental uncertainties.

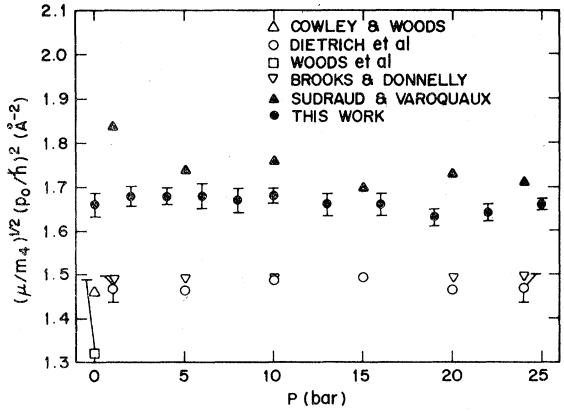

FIG. 21. Parameter $\mu^{1/2}p_0^2$ vs pressure. The open symbols correspond to neutron scattering values; the closed symbols to thermodynamic results. The references are listed in Fig. 20.

To be noted again, the uncertainties quoted in Table II correspond to statistical errors. The total uncertainty in each of the parameters, which includes contributions due to possible systematic errors in the data, is difficult to estimate, and because of the large number of adjustable parameters, may be considerably larger than the standard errors listed.

Analysis 3. To probe the discrepancy between the neutron and thermodynamic roton parameters further, this set of fits was run with Δ held fixed at the zero-temperature values derived from the neutron data by Brooks and Donnelly.[28] D was fixed at zero, and A, C, E, and F were treated as adjustable parameters. The results are listed in Table II. A vapor pressure constraining Δ to 8.71 K, which is about 0.1 K smaller than the best-fit value determined in analysis 2, resulted in an increase of only 20% in the rms deviation. Thus it is nearly possible to completely compensate for this constraint placed on Δ by adjustments in the remaining parameters, particularly, as expected, in the parameter F. However, the most recent and presumably the most accurate neutron data[27] obtained at 0.75 K yield a vapor pressure Δ of only 8.618 ± 0.009 K. Constraining Δ to this value causes the rms deviation to be increased by nearly a factor of 2 and it becomes more difficult to argue that the present specific-heat results at $P=0$ are consistent with the neutron data. At higher pressures the discrepancy becomes more apparent. Relative to the results of analysis 2, the rms deviation at 25 bars is more than a factor of 4 larger. It should also be noted that (i) the sound velocities yielded by this analysis are significantly too high at the higher pressures; (ii) α_2 changes sign near 10 bars in disagreement with other experiments; (iii) α_4 decreases extremely rapidly with increasing pressure, implying an unrealistic dispersion relation at high pressure; and (iv) there are large systematic deviations of the data from the fitting function which result in best-fit parameters which depend strongly on T_{max}. In Fig. 22(a) the measured roton specific heat, i.e., the total specific heat minus the phonon contribution (analysis 2), is compared with that calculated using Eq. (7) and the zero-temperature roton parameters determined from the neutron scattering experi-

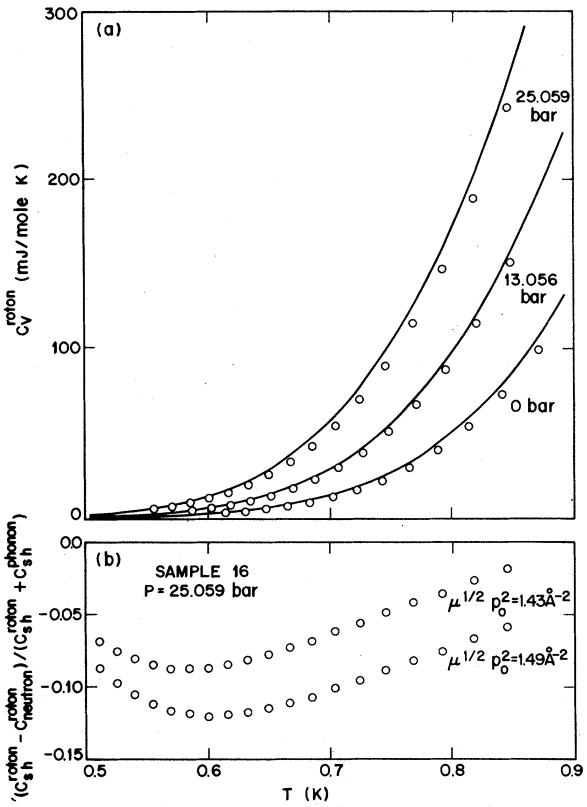

FIG. 22. (a) Roton specific heat vs temperature for three sample pressures. The solid lines correspond to the specific heat computed using Eq. (7) and roton parameters determined from neutron scattering measurements. The symbols correspond to the total measured specific heat minus the phonon contribution. (b) The relative difference between the computed and measured specific heat at 25 bars for two values of the parameter $(\mu/m_4)^{1/2}(p/\hbar)^2$.

ments. At $P=0$, 13.056, and 25.059 bars, the respective values of Δ, 8.61, 7.85, and 7.22 K were used. For each of the pressures $(\mu/m_4)^{1/2}(p_0/\hbar)^2$ was set equal to 1.49 Å^{-2}. At $P=0$, the deviations are nearly proportional to C_V^{roton} and can be reduced considerably by using a smaller effective mass for the rotons which is still consistent with the neutron data. The agreement is improved further, as indicated by the results listed in Table II, by a small adjustment of phonon specific heat. At the higher pressures the deviations are definitely not proportional to C_V^{roton} and thus changing the effective mass will not significantly improve the agreement. The deviations of the 25-bar data relative to the total specific heat are shown in Fig. 22(b) for two values of $\mu^{1/2}p_0^2$. At 0.6 K the discrepancy amounts to roughly 10% of the total specific heat. The phonons make up about $\frac{1}{3}$ of the total specific heat at this temperature. Thus if the discrepancy were to be attributed to an improper subtraction of the phonon contribution, this term would have to be in error by 30% at this temperature (and by 75% at 0.7 K). We thus rule out this possibility.

The effects of the deviations from a parabolic roton minimum were also considered. Approximating the energy in this region of the spectrum by

$$\epsilon = \Delta + (p-p_0)^2/2\mu + \beta(p-p_0)^3/2\mu p_0 \qquad (10)$$

with $\beta > 0$, the specific heat is given by the relation[30]

$$C_V^{roton} = F\left(\frac{\Delta}{k_BT}\right)^{3/2}\left[1+\frac{k_BT}{\Delta}\left(1-\frac{3\beta\mu\Delta}{p_0^2}\right)+\frac{3}{4}\left(\frac{k_BT}{\Delta}\right)^2\left(1-\frac{6\beta\mu\Delta}{p_0^2}\right)\right]e^{-\Delta/k_BT}. \qquad (11)$$

Thus adding the $(p-p_0)^3$ term does decrease the specific heat computed from the neutron data. However, this correction is nearly a linear function of the temperature and amounts to only ~1% at $k_BT/\Delta = 0.1$. In addition, this decrease will be at least partially offset by the positive contribution due to the term in $(p-p_0)^4$.

Of course, including the very small contributions to the specific heat due to the maxons or to the region of the spectrum beyond the roton minimum can only increase the difference plotted in Fig. 22(b). Therefore, ruling out the possibility of large errors in the high-pressure neutron data or in the extrapolation of these results to low temperature, there is a significant discrepancy between the two types of measurements. Sudraud and Varoquaux[29] interpret the discrepancy between the neutron and thermodynamic roton parameters as providing evidence for the existence of interactions between rotons and virtual excitations.

Analysis 4. In each of the previous analyses the series approximation of the ϵ-p dispersion relation was assumed to contain only odd powers of the momentum p, and thus the coefficients of the T^4 and T^6 terms in the expression [Eq. (4)] for the specific heat were set equal to zero. However, Kemoklidze and Pitaevskii[31] and Feenberg[32] have shown that because of the long-range Van der Waals interaction between helium atoms there is a term in the energy expression proportional to p^4. These authors find that

$$\alpha_3 = \pi^2\phi p/24m_4^2c_0^2, \qquad (12)$$

where the long range part of the Van der Waals potential between a pair of helium atoms is ϕ/r^6. At $P=0$ this expression implies $\alpha_3 = 3.34$ Å^3 and

thus for $P \geq 0$, α_3 (in Å^3) can be computed using $\alpha_3(P) = 3.34V(0)/V(P)[c_0(0)/c_0(P)]^2$.

Following Berthold *et al.*,[22] we have assumed in this analysis that this is the only contribution to α_3. The parameter D for each pressure was thus fixed at the appropriate value determined using Eqs. (4) and (12). The remaining parameters A, C, E, F, and Δ were adjustable. The data were fitted over the same temperature range used in analyses 2 and 3. The results are given in Table II. Each of the tabulated values of α_3 differs slightly from the value determined using Eq. (12). This is due to the fact that in computing the fixed values of D, values of the sound velocity (analysis 1) were used which differ from the best-fit values resulting from this analysis. These latter velocities were used in converting D back into listed values of α_3. The constraint placed on D does not lead to a significant change in the rms deviation for any of the samples and is therefore consistent with the data. We also note that the roton parameters are essentially the same as those resulting from analysis 2. The values of c_0, α_2, and α_4 are compared with the respective values determined in the previous analyses in Figs. 18, 17, and 19. The present analysis yields sound velocities which are in the closest agreement with the ultrasonic data. At $P = 0$, $\alpha_2 = -1.55$ Å^2, in excellent agreement with the value determined by Berthold *et al.*,[22] namely, -1.7 ± 0.34 Å^2. As noted earlier, these authors also used the theoretical value for α_3 in their analysis of thermal expansion measurements. The inclusion of the T^6 term pushes P_c to a slightly higher pressure but it still remains in the vicinity of 20 bars and is therefore consistent with the sound propagation experiments.

The form of the dispersion relation described by the parameters determined in this analysis of the specific heat data is shown in a sensitive manner in Fig. 23 for several pressures. Actually plotted

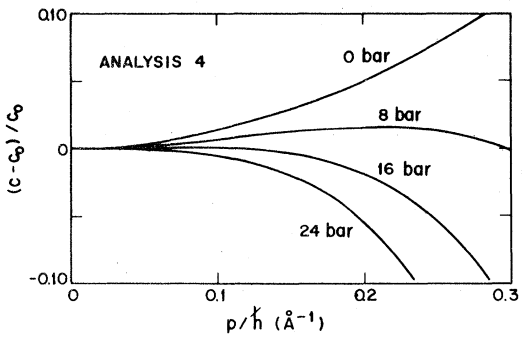

FIG. 23. Relative change in the phonon phase velocity, computed using the parameters determined in analysis 4, as a function of the phonon momentum.

is the relative change in the phonon phase velocity ($c \equiv \epsilon/p$) computed using the relation

$$\frac{c - c_0}{c_0} = \frac{-\alpha_2}{\hbar^2} p^2 - \frac{\alpha_3}{\hbar^3} p^3 - \frac{\alpha_4}{\hbar^4} p^4 . \tag{13}$$

Analysis 5. In analyses 1–4 it was assumed that the expression for the specific heat derived under the assumption that the phonons are noninteracting properly describes the situation in liquid helium. Phonon-phonon interactions lead, however to quasiparticles with finite lifetimes and thus the expression relating the specific heat to the dispersion curve must be in some way modified. It is not clear though what the leading temperature dependence of the lifetime correction δC_v should be. Most estimates[30,33,34] indicate that $\delta C_v \sim T^7$ or T^9. A microscopic analysis by Wong and Gould,[34] however, yields the result that for an interacting Bose liquid the leading, low-temperature correction to the specific heat is

$$\delta C_v = -0.035 g^2 \frac{15}{2\pi^2} A \frac{T^5}{T_0^2} \ln \frac{T_0^4}{gT^4} , \tag{14}$$

where A is defined in Eq. (5) and $T_0 \equiv m_4 c_0^2/k_B$. Assuming that this relation is also valid for helium then at vapor pressure $T_0 \approx 28$ K, and g is estimated to be about 6.3. These parameters imply that in the temperature range 0.1–0.8 K, δC_v is on the order of several percent of CT^5 (using values of C from Table II), and changing in relative size slowly with temperature. Thus this contribution to the specific heat is extremely difficult to distinguish experimentally from the T^5 term. At 20 bars, the estimated magnitude of δC_v is considerably smaller than the uncertainty in the CT^5 contribution determined in analysis 4. The situation is even more complicated due to the fact that it is the lowest-temperature data which would be most useful in determining if this term is actually present and it is these data which are most sensitive to the precise choice of δ (see Sec. III A) used in the calibration of the thermometers. Nonetheless, the term $GT^5 \ln T$ was added to the fitting function and several fits were run principally to determine if this could produce any significant change in the roton parameters. In the first set of fits A, C, E, F, D, and G were treated as adjustable parameters, and D was fixed at its theoretical value. The best-fit values of both F and Δ were, as expected, essentially the same as those yielded by analyses 2 and 4. The only change made in the second set of fits was to fix Δ to agree with the neutron data. As in analysis 3, fixing D resulted in extremely poor fits with rms deviations increasing rapidly with increasing pressure.

IV. SUMMARY

High-precision measurements of the low-temperature specific heat of high-purity liquid ^{4}He were made at eleven molar volumes corresponding to the pressure range from 0 to 25 bars. The data were obtained between 65 and 850 mK, using a large, thin-walled copper sample chamber which was thermally well isolated and which was filled with the helium samples via a quartz capillary. A valve located on the mixing chamber of the dilution refrigerator was used to confine the samples to constant volume.

The specific-heat data at the lowest temperatures are sensitive to the exact choice of δ (in the CMN susceptibility-T relation) used in calibrating the working thermometers. The constant δ was taken to be equal to 2 mK since this assumption leads to low-temperature specific-heat results for each sample, which can be described well by a function of the form AT^3+CT^5; this is consistent with the implications of high-precision ultrasonic measurements. Several different analyses were performed on these data. Each indicated that the phonon dispersion is anomalous at low pressure and becomes normal above roughly 16 bars, in agreement with other experiments. Quantitatively, however, the parameter α_2 is sensitive to the functional form used in fitting the data. The best results were obtained using a relation which contained T^3, T^5, T^6, and T^7 terms to describe the phonon contribution. This set of fits (analysis 4) yielded $\alpha_2=-1.55$ Å^2 at $P=0$, a crossover pressure of about 20 bars, and sound velocities in excellent agreement with the directly measured values.

The specific-heat data also confirm the existence of unexplained discrepancies between roton parameters derived from thermodynamic data and those determined by neutron scattering measurements. The values of Δ resulting from this work are at all pressures approximately 0.2 K larger than the respective neutron values; the quantity $\mu^{1/2}p_0^2$ is about 10% larger than the neutron data at all pressures. These discrepancies are outside of the combined experimental uncertainties and are contrary to the principle assumptions of the Landau theory. It is thus important that this problem be resolved.

The data for the high-purity ^{4}He samples ($\delta=2$-mK thermometer calibrator) are available in numerical form.[35]

ACKNOWLEDGMENTS

I am grateful to F. V. DiMarcello for preparing the quartz capillary, to H. Meyer for suggesting the use of the self-inductance CMN susceptibility bridge, and to P. R. Roach for supplying drawings of the cold valve. I am also grateful to G. Ahlers, R. P. Behringer, R. N. Bhatt, and P. C. Hohenberg for helpful discussions, and to P. A. Busch for technical assistance.

APPENDIX

To facilitate the determination of the specific heat, or other thermodynamic functions, at any molar volume the following relations are provided:

$$V\ (\mathrm{cm}^3)=27.555406-0.30624450P+8.2676220\times10^{-3}P^2-1.1743928\times10^{-4}P^3$$

$$c_0\ (m/\mathrm{sec})=239.59052+7.7187795P-0.16440605P^2+2.3701258\times10^{-3}P^3$$

$$\alpha_2\ (\text{Å}^2)=-1.268+0.0577P$$

$$\alpha_3=0$$

$$\alpha_4\ (\text{Å}^4)=4.022+1.060P$$

$$\Delta\ (K)=8.8055902-0.067057902P+4.3252224\times10^{-4}P^2$$

$$(\mu/m_4)^{1/2}(p_0/\hbar)^2\ (\text{Å}^{-2})=1.66$$

The specific heat values computed using Eqs. (5) and (7) and these expressions agree to within 1.5% with the high-purity ^{4}He data presented in this paper.

[1]H. J. Maris, Rev. Mod. Phys. 49, 341 (1977), and references therein.
[2]H. J. Maris, Phys. Rev. A 8, 2629 (1973).
[3]R. K. Wehner, Phys. Rev. A 9, 2625 (1974).
[4]P. F. Meier, H. Beck, and R. Beck, Phys. Rev. B 12, 3745 (1975).
[5]P. R. Roach, J. B. Ketterson, B. M. Abraham, and M. Kuchnir, J. Low Temp. Phys. 9, 105 (1972).
[6]W. R. Junker and C. Elbaum, Phys. Rev. B 15, 162 (1977).
[7]N. E. Phillips, C. G. Waterfield, and J. K. Hoffer, Phys. Rev. Lett. 25, 1260 (1970).
[8]P. R. Roach, J. B. Ketterson, and M. Kuchnir, Rev. Sci. Instrum. 43, 898 (1972).
[9]D. S. Greywall, Phys. Rev. B 15, 2604 (1977); 16, 5129(E) (1977).
[10]Brazing alloy: 72% silver, 28% copper.
[11]B. M. Abraham, Y. Eckstein, J. B. Ketterson, M. Kuchnir, and P. R. Roach, Phys. Rev. A 1, 250 (1970).
[12]E. C. Kerr and R. D. Taylor, Ann. Phys. 26,

292 (1964).
[13]United States Bureau of Mines, Helium Operations, Amarillo, Texas.
[14]G. J. Sellers and A. C. Anderson, Rev. Sci. Instrum. 45, 1256 (1974).
[15]B. M. Abraham and Y. Eckstein, Phys. Rev. Lett. 20, 649 (1968).
[16]A. C. Anderson, J. Appl. Phys. 39, 5878 (1968).
[17]P. R. Roach, B. M. Abraham, J. B. Ketterson, and M. Kuchnir, Phys. Rev. Lett. 29, 32 (1972).
[18]P. J. Bendt, R. D. Cowan, and J. L. Yarnell, Phys. Rev. 113, 1386 (1959).
[19]O. W. Dietrich, E. H. Graf, C. H. Huang and L. Passell, Phys. Rev. A 5, 1377 (1972).
[20]R. A. Sherlock, N. G. Mills, and A. F. G. Wyatt, J. Phys. C 8, 2575 (1975).
[21]R. C. Dynes and V. Narayanamurti, Phys. Rev. B 12, 1720 (1975).
[22]J. E. Berthold, H. N. Hanson, H. J. Maris, and G. M. Seidel, Phys. Rev. B 14, 1902 (1976).
[23]B. M. Abraham, Y. Eckstein, J. B. Ketterson, and J. M. Vignos, Phys. Rev. Lett. 16, 1039 (1966).
[24]J. Jäckle and K. W. Kehr, Phys. Rev. Lett. 27, 654 (1971).
[25]P. R. Roach, J. B. Ketterson, and M. Kuchnir, Phys. Rev. Lett. 25, 1002 (1970).
[26]R. A. Cowley and A. D. B. Woods, Can. J. Phys. 49, 177 (1971).
[27]A. D. B. Woods, P. A. Hilton, R. Scherm, and W. G. Stirling, J. Phys. C 10, 45 (1977).
[28]J. S. Brooks and R. J. Donnelly, J. Phys. Chem. Ref. Data 6, 51 (1977).
[29]M. Sudraud and E. J. Varoquaux, Phys. Lett. A 62, 416 (1977); M. Sudraud, Ph.D. thesis (Orsay, 1977) (unpublished).
[30]R. N. Bhatt (private communication).
[31]M. P. Kemoklidze and L. P. Pitaevskii, Zh. Eksp. Teor. Fiz. 59, 2187 (1970) [Sov. Phys. JETP 32, 1183 (1971)].
[32]E. Feenberg, Phys. Rev. Lett. 26, 301 (1971).
[33]I. M. Khalatnikov, in *The Physics of Liquid and Solid Helium, Part I,* edited by K. H. Bennemann and J. B. Ketterson (Wiley, New York, 1976).
[34]V. K. Wong and H. Gould, Phys. Rev. B 14, 3961 (1976).
[35]See AIP document No. PAPS PLRBA-18-2127-11 for 11 pages of tabulated data. Order by PAPS number and journal reference from American Institute of Physics, Physics Auxiliary Publication Service, 335 East 45th Street, New York, N.Y. 10017. The price is $1.50 for each microfiche (98 pages), or $5.00 for photocopies of up to 30 pages with $0.15 for each additional page over 30 pages. Airmail additional. Make checks payable to the American Institute of Physics. This material also appears in *Current Physics Microfilm*, the monthly microfilm edition of the complete set of journals published by AIP, on the frames immediately following this journal article.